

OPEN ACCESS

Electric fuses operation, a review: 2. Arcing period

To cite this article: W Bussière 2012 *IOP Conf. Ser.: Mater. Sci. Eng.* **29** 012002

View the [article online](#) for updates and enhancements.

You may also like

- [Experimental study of HBC fuses working at short and medium pre-arcing times](#)
W Bussière, D Rochette, G Velleaud et al.
- [Dynamic physical characteristics of DC arc on arcing horn for HVDC grounding electrode line](#)
Yicen LIU, , Chenguang YANG et al.
- [Impact of arcing on carbon and tungsten: from the observations in JT-60U, LHD and NAGDIS-II](#)
Shin Kajita, Masakatsu Fukumoto, Masayuki Tokitani et al.



ECS
The
Electrochemical
Society
Advancing solid state &
electrochemical science & technology

DISCOVER
how sustainability
intersects with
electrochemistry & solid
state science research

Electric fuses operation, a review: 2. Arcing period

W Bussière

Clermont Université, Université d'Auvergne, LAEPT, BP 10448, F-63000 Clermont-Ferrand, France

E-mail: william.bussiere@univ-bpclermont.fr

Abstract. In the electric fuse operation the arcing period follows immediately the pre-arcing period depicted in Part 1 (*Part 1. Pre-arcing period*). The transition between these two operation steps is not fully understood at this time. To simplify the beginning of the arcing period can be identified with the electric arc ignition i.e. with the electrodes voltage drop. The consecutive plasma is of metallic type at the beginning of the arcing period and of metallic plus silica type with varying mixture up to the end of the arcing period. The energy brought by the fault current is withdrawn by means of the interaction between the electric arc and the arc quenching material (usually silica sand) whose morphometric properties influence the properties of the plasma column: composition, thermodynamic properties and transport coefficients of the plasma column depend on the porosity (and other morphometric properties) of the filler. The fuse element erosion also known as burn-back is responsible for the lengthening of the plasma column and the variations of the electric field. The whole of these processes is depicted by means of experimental results or modellings when possible.

1. Introduction

In spite of their apparent simplicity both for technical, geometrical and working considerations the physical processes involved in electric fuse operation are far to be fully understood. Moreover they are of very high interest for electrical safety purposes both for persons and systems and widely used in the Low and Middle Voltage systems.

Some general considerations linked to the *arcing* period from the electrical and physical point of views are given in the Part 1 (*Part 1. Pre-arcing period*) of the current review. Especially the *arcing* period in its whole is described from the chemico-chemical point of view.

During the *arcing* period the energy brought by the *fault* current has to be dispersed on one hand. And the electric field induced by the plasma column has to shorten the *arcing* period duration on the other hand. A long *arcing* time is problematic because the electrical conductivity of the plasma column is high enough to allow the flow of the *fault* current and can induce irreversible damage in the devices behind the point of the *fault* current appearance. The electric field (E) level of the plasma column necessary to ensure a short *arcing* time is the result of the compromise between the increase of the voltage across the fuse (v_f) and the relative limitation of the plasma column lengthening or inter-electrodes gap (d_{ie}). In other words the most favourable situation is to quickly increase the electric fuse voltage so that it can not be maintained any more by the supply thus forcing the current to fall down. If one considers that $v_f \approx E \times d_{ie}$ it follows two main remarks. First the electric field of the plasma column is the result of the chemical species issued from the melting and the vaporization of the

metallic (mainly silver) fuse element and from the melting and the vaporization (and the dissociation of various chemical species produced at low temperature in the plasma) of the silica sand. The density of each of these chemical species varies inside the plasma volume and also during the *arcing* period. Consequently the electric field varies on the whole duration of the electric fuse operation and can be strongly inhomogeneous from the centre to the edges of the plasma column because of material (silver and silica) injection. Secondly the length of the plasma column which is roughly the gap between the two erosion fronts of the fuse element increases during the *arcing* period. The erosion of the fuse element is the result of various parameters. The fuse element features (material, thickness, shape of the reduced section, number and distribution of the reduced sections on the whole length of the fuse element), the *fault* current level, the level of di/dt at the *fault* current appearance, the energy transfer from the plasma column later during the *arcing* period are some of the main parameters. The selected set of these parameters has to be chosen in order to increase the length of the plasma column at the maximum. But there is a high limit: one has to prevent the merging of each of the plasma columns appearing around each reduced section. If not the electric fuse can be considered as a single plasma column on the whole length of the fuse element which could lead to the electric fuse destruction.

It is not possible to give a full depiction of the physical processes occurring during the *arcing* period by means of a single tool such as a modelling especially as these processes are not still well known or identified. Section 2 is organized as follows. The problematics of the *arcing* period depiction is discussed in section 2.1. Phenomena occurring around the erosion fronts are addressed in section 2.2. Section 2.3 is dedicated to the study of the plasma column, especially the *burn-back* rate, the assessment of some plasma column properties such as the plasma composition, the plasma radiation, the temperature and the electron density, and the *fulgurite*. The comparative analysis of these properties is done in section 2.4. Section 2.5 is dedicated to the trends in electric fuse modelling for the *arcing* period.

2. Arcing phenomena in electric fuses

2.1. Which depiction for which phenomenon?

Arcing period understanding is a very complex task. Many approaches are carried on with plus or less success depending on the expected level of physical depiction.

Difficulties lie in various problematics: the simultaneity of various physical mechanisms occurring in the whole of the interaction volume or are confined either in the plasma column either around the close surroundings of electrodes (with a differentiation between cathode and anode phenomena) ; the very strong gradients – in temperature, electron density and pressure – from the core of the plasma column to the surroundings causing fluctuations in the dependent transport coefficients such as electrical conductivity, thermal conductivity, viscosity and radiation ; the two main materials - silver and silica – in the solid, liquid and vapour phases ; a continuously varying plasma composition resulting from material ablation – erosion of the fuse element also called *burn-back* and ablation of the silica sand grains – and material removal – spreading of liquid silica through the filler interstices, condensation of metallic vapours in the plasma surroundings – from the plasma core.

To be understood each of these problematics was first studied separately if possible and mainly by experiments. With these experimental databases empirical formulations or modellings were produced but often with significant limitations implying new experiments to obtain the value of adjustable parameters. The next step consisted in semi-empirical modellings or physical modellings dedicated to *arcing* period in its whole. In this latter case the contribution of experimental results is required for comparison purposes.

2.2. Cathode and anode phenomena

As for another types of arc discharges one has to take into account phenomenas occurring at the arc roots. General considerations about arc roots can be found in [1, 2], and cathode and anode phenomena are reviewed respectively in [3, 4] and [5-7] with a detailed review of experimental and

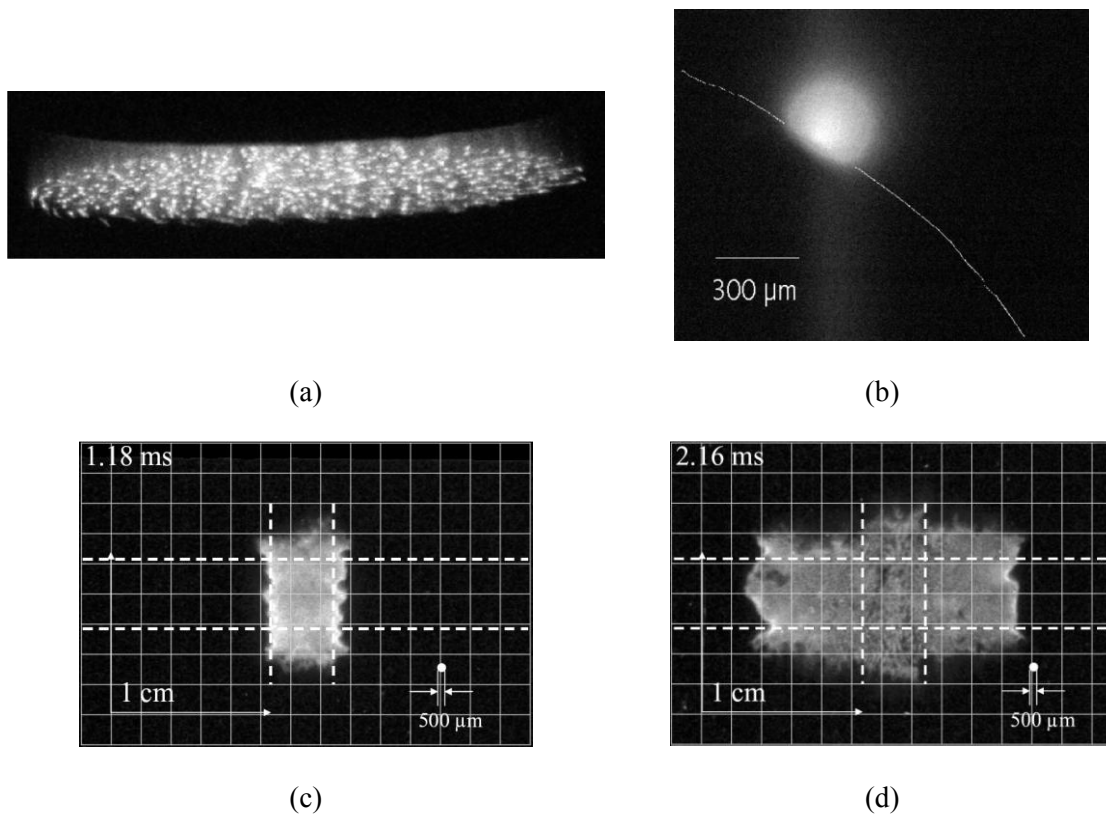


Figure 1. Pictures of arc roots obtained by high-speed imagery (see quoted references for full details). (a) Cathode spots view in the case of high-current (11 kA) developed vacuum arc stabilized by axial magnetic field (0.25T), exposure 25 μs (copper-chromium electrodes) [6]. (b) Side-on view of a cathode spot on a hot tungsten cathode (thin curved line) at 1.3 bar argon and 1 A current, exposure 500 μs (band-pass filter at 4008.nm suppressing argon lines) [3]. (c), (d) Silver fuse element strip (~ 5 mm-width, 2 circular reduced sections) view focussed on the reduced sections area, $di/dt \sim 2 \times 10^6 \text{ A}\cdot\text{s}^{-1}$, exposure 3.8 μs (band-pass filter centered on Ag I 520 and Ag I 546 nm) respectively obtained 1.18 ms and 2.16 ms after the start of the *fault* current, *pre-arcing* time ~ 0.89 ms (dashed lines symbolize the initial position of the fuse element strip) [12].

theoretical studies. There exist only few works dealing with cathode and anode phenomena dedicated to electric fuses [8-10]. These latter include the cathode and anode regions in a theoretical approach with simplifying assumptions.

No specific experimental studies are dedicated to arc roots or more exactly to erosion fronts in the case of electric fuses: one of the main difficulties lies in the shifting of the two erosion fronts during the *arcing* period. To illustrate the very high difficulty to assess experimentally these phenomena even in the case of motionless electrodes we refer to figures 1(a) and 1(b) for cathode views. Figure 1(a) refers to a high-current vacuum arc whose ignition takes place on cold electrodes. As mentioned in [6] during the whole duration of an arc (\sim ms) the cathode spots (bright points in figure 1(a)) appear, growth and hence disappear many times. During its life each cathode spot is the area where electrode material is removed (inside the cathode spot the temperature is higher than the boiling temperature) to form the plasma by means of plasma jet and microdroplets. The significance of these processes depends on the electrode material, the current and the duration of the arc. In figure 1(b) is shown a side-on view of a spot on a hot cathode in the case of an argon arc with a hot tungsten cathode. As quoted in [3] the bright spot can be seen on the surface of the cathode and its position changes by

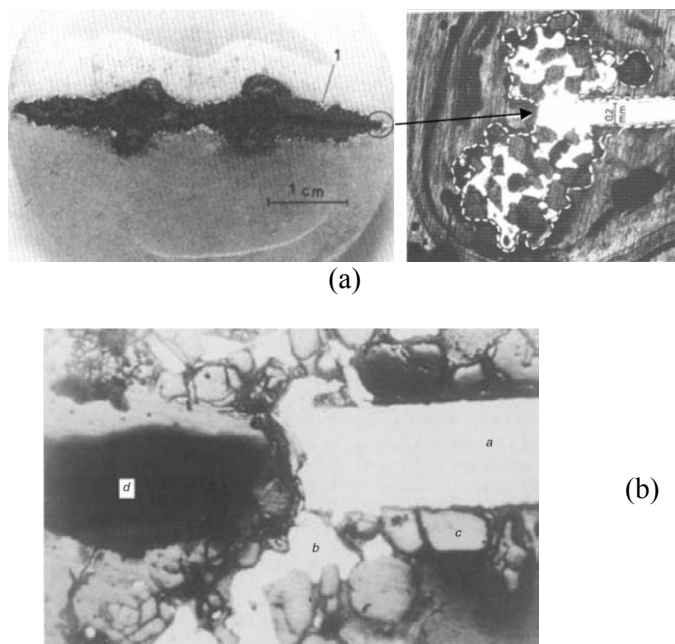


Figure 2. (a) Cross-section of a fulgurite cut along the arcing channel axis, copper fuse element with two reduced sections : 1, copper droplets ; circle fuse element end directly in contact with the arc column (metal droplets in white, sand grains in grey) [13]. (b) Microscopic picture of fulgurite section from *Wright et al.*: a, electrode ; b, electrode material which has flowed away in liquid form ; c, grains of filler ; d, arc cavity which has been filled with araldite to enable the section to be made through the fulgurite [9].

jumps of the order of 100 ms. As a consequence of these two latter quotations one understands that the erosion fronts in a fuse can be seen as a combination of all these features.

An example of the erosion fronts in a silver fuse strip is shown in figures 1(c) and 1(d). These two frames are extracted from a high-speed film for the times 1.18 ms and 2.16 ms, the *pre-arc* duration ~ 0.89 ms, the time of measurable intensity ~ 3.61 ms, $di/dt \sim 2 \times 10^6$ A·s⁻¹, Joule integral $\sim 6.2 \times 10^3$ A²·s, and the observed spectrum is restricted to those including the two neutral silver lines at 520 nm and 546 nm (to be disturbed the less possible by the radiation issued from silicon lines). In the used camera pictures are focussed on a black and white photographic film. Figure 1(c) shows that ~ 300 μ s after the arc ignition (sharp increase of the voltage across the fuse) which is close to the peak fuse current (~ 2.1 kA) the inter-electrodes gap is ~ 4.6 mm and that the two erosion fronts are erratic with roughly half-circular shapes for the irregularities distributed along the fuse element strip width. It has to be noticed that metallic vapours spread in the width direction further away from the initial position of the fuse strip. Figure 1(d) is observed ~ 1.3 ms after the arc ignition *i.e.* during the decrease of the fuse current. Erosion fronts are more regular without showing a clear trend. Some gradients in intensity are observed in the whole of the interaction volume with strong inhomogeneities right in the centre. Especially at the cathode side (left part in figure 1(d)) it can be seen a highly irregular erosion front.

Keeping in mind the previous remarks – especially the considerations given to explain the observed fluctuations – and the pictures shown in figures 1(c) and 1(d) we understand that a thorough investigation of the arc roots in a fuse or at least of the erosion fronts is made more complex by the instability of the erosion fronts and the time-changing shape. So there remains a non negligible lake of knowledge which could be very helpful to understand better the transition between the *pre-arc* and the *arc* periods.

2.3. Burn-back and growth of the plasma column

2.3.1. Burn-back rate. The erosion of the fuse element also called *burn-back* has been widely studied within the electric fuse community. Many experimental studies and modellings can be found in the literature [14].

The initial point of the *burn-back* approach can be seen in figure 2(b) and also in figure 11(b) (*Part 1. Pre-arc period*): at the solid fuse element end some liquid silver splashings can be seen starting

from the liquid-vapour erosion front. It is interesting to note that in the two pictures the liquid splashing is seen flowing through the interstices which would lead to assume a high level of pressure linked to the vaporization: it is clearly shown in figure 2(a) close to the fuse element end. This indicates that only a part of the fuse element is vaporized to form the plasma column: this would seem to confirm the assertion quoted in section 2.2 about *microdroplets* but at another scale and raises the problem of the vaporized part of the total fuse element material. *Wright et al.* [9] gives the following relation for the vaporized mass (m_v) as a function of the total mass (m_t): $m_v/m_t = 40\%$ which results from many actual fuse tests. To assess the inter-electrodes gap or *burn-back* length equality is assumed between the energy provided for melting and vaporisation:

$$E_{MV} = 2 \times (V_{af} + V_{wf} + V_T) \times \int_0^{t_{arc}} i(t) \cdot dt$$

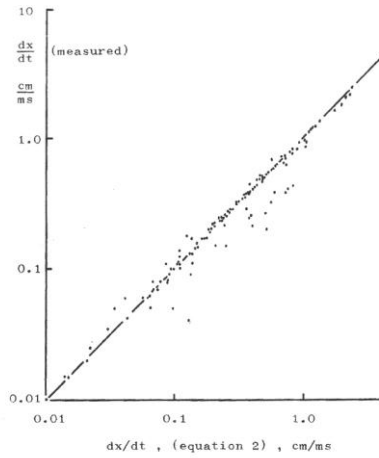
(V_{af} : voltage of anode fall, V_{wf} : work function equivalent voltage of the fuse element material, V_T : voltage associated with the thermal energy of the electrons which enter the anode), and the energy necessary to remove electrode material: $E_{MV} = m_t \times L_m + m_v \times L_b + m_t \times (T_m - 200) \times c_s$ where 200°C is the bulk temperature raise of the electrode material during the *pre-arc* period. So doing the energy necessary for the temperature increase from melting to boiling point is neglected.

From these bases two other main calculations are done: the cross-sectional area of the positive column and its electrical conductivity. Many simplifying assumptions are done and justified keeping in mind that the complexity of physical processes in a fuse prevents a full modelling of the fuse arc [9]. We highlight two problematics.

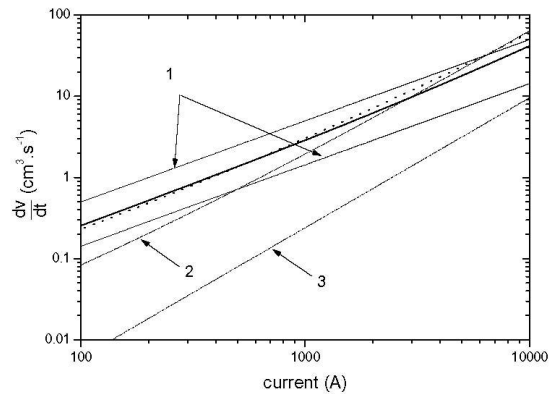
First both for electrons and atoms the Maxwell distribution for velocity is assumed valid. Respectively for the kinetic energy (E_{ai}) of atoms/ions (n_{ai}) which are scattered out of the column and for the kinetic energy (E_e) of the electrons (n_e) scattered out of the column *Wright et al.* write: $E_{ai} = 3/2 \times n_{ai} k_B T$ and $E_e = 3/2 \times n_e k_B T$, where T is the mean temperature defined for a step time in the calculation. These two latter formulas imply the same temperature for electrons (T_e) and heavy particules (T_h) that is to say that thermal equilibrium is checked [15]. This assumption can be reasonably accepted for the core of the plasma column *i.e.* far from the edges where material is injected by means of liquid silica vaporization and where the pressure is the highest. On the contrary it is rather questionable for volumes close to the silica liquid/vapour interface (plasma column surroundings) and close to the silver liquid/vapour interface namely the fuse element ends.

Secondly electrical conductivity (σ) is assessed from the Spitzer's formula written for ionisation levels of more than 0.01%, the electron density being deduced from Saha's equation assuming that $n_e = n_i$. As previously this can be properly assumed for the plasma core. But it is more questionable for the periphery of the plasma core because of the strong gradients for temperature, pressure and density moreover as material injection changes the plasma composition during the whole of the fuse operation. As a matter of fact we recall that σ follows roughly the electron density as n_e^2 [16]: small variations of the metallic material amount vaporized to form the fuse plasma can imply strong variations of the resulting electron density [17].

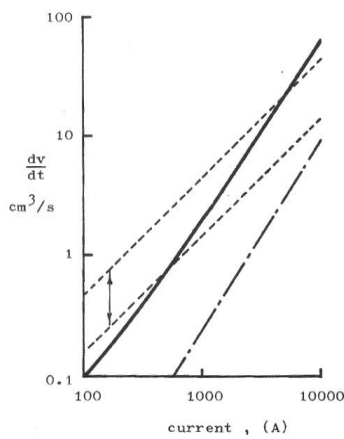
Empirical formulas deduced from many experiments have been published in [18]. The *burn-back* rate is deduced by assuming that the fuse element erosion is mainly due to local electrode effects. The temperature of metal droplets is obtained from the comparison between experimental *burn-back* rate and empirical values calculated from the latter consideration: 1700 K for silver droplets and 1356 K for copper droplets. From [19] a useful formulation is given for the *burn-back* rate (figure 3(a)): $dx/dt = 10^{-4} \times (4.6 + 0.236 \times i^{0.6}) \times i/S$ where $i = i(t)$ (A) and S (cm²) is the cross-section area. This formulation improves the older reliability obtained with linear approximation. For the volumetric erosion rate *Wilkins et al.* give: $dv/dt = 10^{-4} \times (4.6 \times i + 0.236 \times i^{1.6})$ cm³·s⁻¹. It is compared in figure 3(b) with the results of *Turner et al.* [20] where the volumetric erosion rate is studied in the case of



(a)



(c)



(b)

Figure 3. (a) Erosion rate: correlation between experimental results and $dx/dt = 10^{-4} \times (4.6 + 0.236 \times i^{0.6}) \times i/S$ [19]. (b) Volumetric erosion rate versus current: - - -, range of linear approximation ; —, $dv/dt = 10^{-4} \times (4.6 \times i + 0.236 \times i^{1.6})$ [19] ; - · - · -, approximation from [20] deduced from contact erosion. (c) Comparison of volumetric erosion rate [12]: at intermediate current levels for silver (- - -) and copper (—), limits deduced from the linear approximation (1), Wilkins *et al* [19] and Turner *et al.* [20].

contact erosion. There is a significant shift between the results because the heat transfer is different for the two situations, heating of contacts and heating of the fuse element erosion fronts. In the first situation a large part of the incoming energy is used in the heating of the contact, the remaining part being used for erosion. In the second situation only a small part of the incoming energy is used in the heating of the fuse element and the significant remaining energy is used for the fuse element erosion. [19]. Another limitation in the trend curves has to be pointed out: the level of current linked to the level of the overcurrent that has to be cut by the fuse. Correlatively to the type of *pre-arcing* period (short, medium and long) one defines small overload current (typically some I_n , the nominal current), medium overload current and high overload current. These definitions depend on the nominal current of the electric fuse, the features of the *fault* current and supply regarding the power factor, the phase angle of the electrical *fault*, current peak and are resumed in [21] (test series at I_1 , I_2 and I_3). In figure 3(c) experimental volumetric erosion rates from [12] fit well with the approximation from [19] for currents higher than ~ 1000 A. For smaller currents down to ~ 100 A there is a significant gap. For smaller overload currents the role played by the filler and the solid parts of the fuse element can not be considered as negligible in the actual thermal transfer: thus discrepancies appear because the Joule integral contribution is divided in the global heat transfer and in the fuse element erosion.

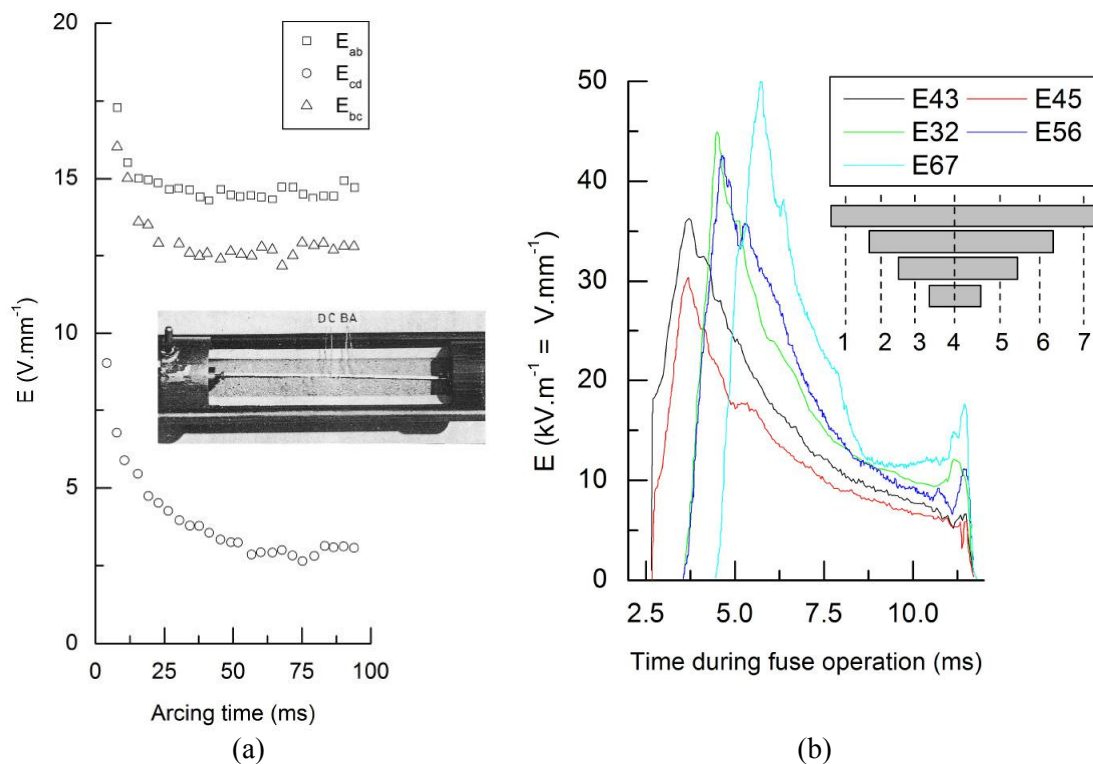


Figure 4. (a) Axial electric field values measured in the case of d.c. arcs in current-limiting fuses [62]. (b) Electric field values measured in the case of HBC fuse tested with high fault current level (1: cathode side, 2: anode side, each probe wire being at 3 mm from adjacent ones) [63].

2.3.2. Plasma column. The formation and the evolution of the plasma column geometry (inner part of the fulgurite obtained after the fuse operation) and of the whole interaction volume (which is assimilated to the whole fulgurite) has been studied experimentally mainly [13, 18, 22] with some attempts to formalize these experimental results in the form of more or less empirical modellings dedicated to the whole of the fulgurite or focussed on the plasma column section also called lumen [9, 10, 18]. This task is of very high difficulty even in the case of experimental results: in an actual fuse the plasma column is enclosed by liquid silica itself enclosed by silica sand grains more or less melted themselves enclosed by solid silica sand grains. As a consequence each experimental attempt can strongly modify the true geometry of the plasma column. In [9] the column is assumed cylindrical for simplifying purposes and the output current and voltage curves obtained by means of the modelling are satisfactory.

The electric field assessment is shown in figure 4 with two different measurements (voltage probes are referenced to earth in both measurements). In figure 4(a) axial electric field values range from $\sim 2.5 \text{ V}\cdot\text{mm}^{-1}$ to $\sim 17.5 \text{ V}\cdot\text{mm}^{-1}$ at the most. These measurements correspond to the average axial electric fields obtained between the probes (nickel alloy probe wires) at positions A, B and C in the case of d.c. arcs in current-limiting fuses. This technique has been fitted to assess the time evolution of average electric field both at the cathode side and at the anode side as shown in figure 4(b) for a total *arcing* period duration ~ 9 ms. Around the centre of the fuse element and on the whole duration of the measurement the evolution of E_{43} is similar to those of E_{45} , the main difference being observed for the peak values at the beginning of the *arcing* period with $E_{43} > E_{45}$. On the contrary as the distance from the centre of the fuse element increases the discrepancies become smaller. The peak values of the

Table 1. Spectroscopic lines from various chemical species observed in the plasma column during the fuse operation, from [25].

3a. Spectroscopic lines		3b. Duration of lines in the arc		
Line	Wavelength (nm)	Wavelength (nm)	Line	Durations (ms)
Ag I	487.410, 520.908, 546.550	441.491	O II	1.924
Si II	504.101, 505.598, 587.376, 595.756, 597.893, 634.710, 637.136	441.698	O II	1.765
Si III	455.262, 456.782, 573.973	455.262	Si III	2.310
O II	418.546, 418.979, 431.714, 433.686	456.782	Si III	2.150
	434.556, 434.943, 436.690, 439.595	466.164	O II	1.820
	441.491, 441.698, 444.821, 445.238	469.921	O II	1.765
	446.628, 446.783, 459.097, 463.885	470.536	O II	1.870
	464.181, 464.914, 465.084, 466.164	487.410	Ag I	0.760
	469.921, 470.536, 492.460, 494.306	504.103	Si II	3.300
		505.598	Si II	3.420
		520.908	Ag I	3.004
		546.550	Ag I	3.180
		573.973	Si III	2.150
		587.376	Si II	3.004
		595.756	Si II	3.100
		597.893	Si II	3.300
		634.710	Si II	3.498
		637.136	Si II	3.498

experimental average electric field range from $\sim 30 \text{ V}\cdot\text{mm}^{-1}$ to $\sim 50 \text{ V}\cdot\text{mm}^{-1}$. Whatever the couple of probe wires or the location of the measurement a regular decrease is observed from the peak value showing that the steady plasma column assumption sometimes made appears to be really questionable. The comparison between the measurements from [62] and [63] can not be done because the fuse elements have different features and are tested in different conditions about the electric *fault*.

The plasma column is now discussed preferentially from the physico-chemical point of view [23]. The first paper dealing with the study of the electric fuse arc plasma has been published by *Chikata et al.* [24]. The main aim of the work is the spectroscopic study – especially Optical Emission Spectroscopy (OES) – of the radiation escaped from the fuse arc plasma: identification of the spectral lines escaped from the plasma column, evolution of the intensity of these lines on the whole duration of the fuse operation and assessment of electron temperature, electron density and ratios of particle densities. This work was done by means of a specific fuse body and a spectrograph equipped with three photomultipliers to observe simultaneously different spectral intervals (use of bandwidth filters) on the whole duration of the fuse operation. A wavelength calibration and a relative intensity calibration were performed. From the time integrated spectra over the 330-560 nm spectral range many lines from different radiated species are identified: Ag I, Si I-II-III (I: neutral, II: first ion, ...) but no lines corresponding to O I-II-III which is due to the studied spectral interval and the value of the energy levels of the excited states for these latter species. It was found a typical temperature $\sim 20\,000 \text{ K}$ and a typical electron density $\sim 10^{18} \text{ cm}^{-3}$. But it has to be noticed that no variation during the fuse operation has been found. Because of the continuously changing radiating volume no Abel inversion was done to obtain the local values of the temperature and the electron density: thus the measurements lead to a mean value or integrated value. On the basis of LTE a set of Saha's equations was built from the experimental relative intensities of the quoted radiated species to calculate the composition and the pressure of the plasma. Stark broadening of ionized silicon lines was also used

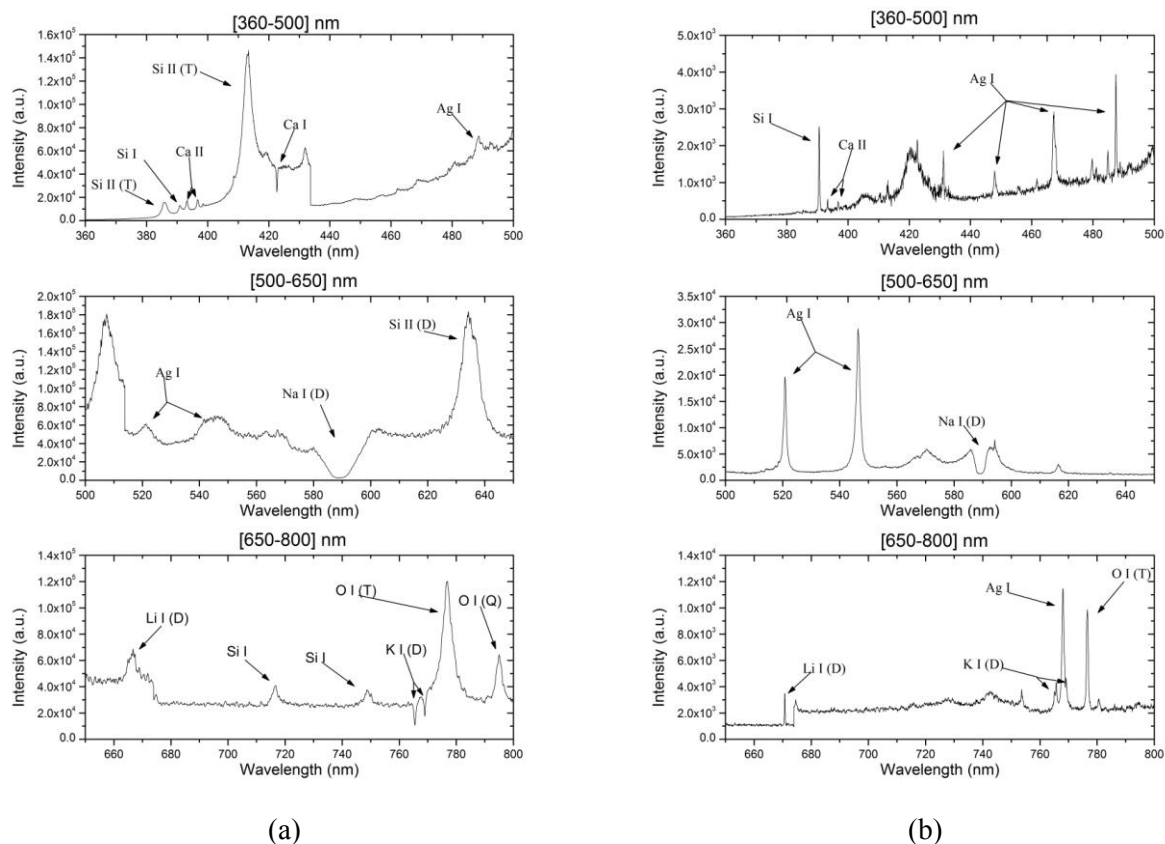


Figure 5. Optical emission spectroscopy dedicated to the fuse arc plasma spectroscopic lines identification [34]: (a) at the beginning of the *arcing* period (~ 0.9 ms) (b) at the end of the arcing period (~ 3.6 ms) in the case of a silver fuse element tested by means of a capacitor bank discharge.

to assess electron density which was compared with values otherwise obtained from composition calculation and experimental line intensity ratios.

This work represents the reference of the later spectroscopic studies: *Stokes AD* and co-workers [25-30] where the *wall-stabilized* interaction dedicated to the fuse arc plasma was tested experimentally and *Cheim* [31, 32]. From these works and [33-36] it appears that the modified fuse body or way to collect the light escaped from the plasma column can influence the results concerning the observation of the ionization degree radiating lines especially as many features – the overload current, the fuse element (geometry and features of the reduced sections and position within the fuse body) and the arc quenching material (chemical features, mean granulometry and packing density) – play a significant role in the resulting temperature, electron density and pressure of the plasma column during the fuse operation [35]. Main trends and results are resumed in the following paragraphs.

We show in table 1(a) the spectroscopic lines observed in [25], the light radiated by the plasma column being directly collected via an optical fibre whose end is inserted very close to the plasma. On the contrary to [24] many O II lines are observed and even some Si III lines which may be attribute to the proximity between the plasma and the optical fibre and electric features. The dependence between the duration of observation, the ionization degree of the chemical species and the implied excitation level is shown in table 1(b). In figure 5 we show the spectra observed by means of a direct integration of the escaped light without any optical fibre inserted in the plasma column, the light being collected by means of a lens from the glass window close to the fuse element to the entrance slit of a spectrometer via an optical fibre [34]. The same chemical species are observed but with a lower ionization degree. By comparison between figures 5(a) and 5(b) the discrepancies between the

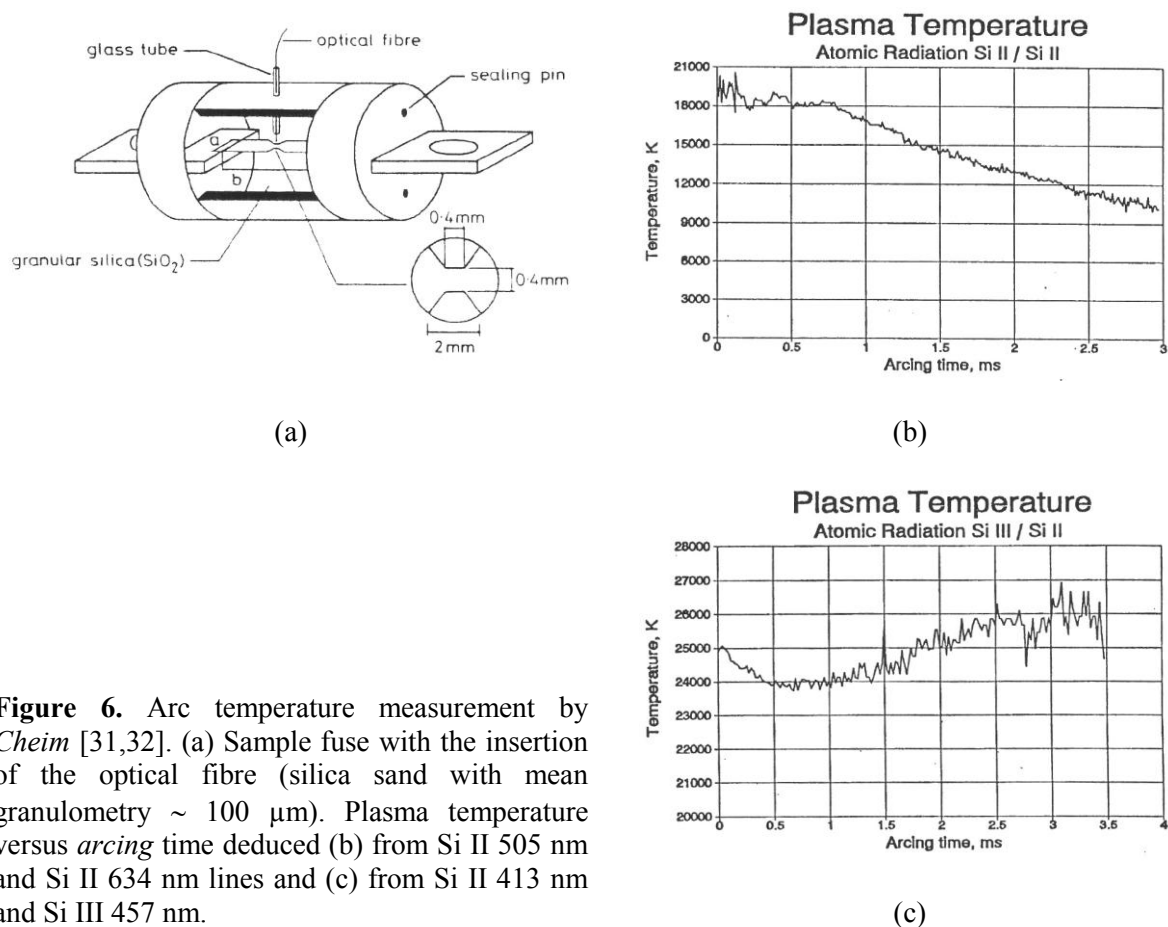


Figure 6. Arc temperature measurement by *Cheim* [31,32]. (a) Sample fuse with the insertion of the optical fibre (silica sand with mean granulometry $\sim 100 \mu\text{m}$). Plasma temperature versus *arcing* time deduced (b) from Si II 505 nm and Si II 634 nm lines and (c) from Si II 413 nm and Si III 457 nm.

radiation observed at the beginning of the *arcing* period (~ 0.9 ms) and at the end of the *arcing* period (~ 3.6 ms) are clear: Si II lines – especially the multiplets Si II (1), Si II (2) and Si II (3) – and O I – especially the triplet ~ 777 nm – show a high level of intensity for ~ 0.9 ms ; on the contrary for ~ 3.6 ms ionized silicon lines are not visible any more, and the spectra are dominated by neutral silicon and silver lines whose excitation energy levels are lower than those of Si II and O I.

The Na I doublet seen ~ 589 nm is due to the nature of the glass window (the same for Li I, Ca I and K I). It was used in [37,38] to study the colder periphery of the plasma column, especially the temperature: in the case of the capillary [37] a temperature ~ 4300 K is found, in the case of the electric fuse [38] a temperature ~ 6600 K is found. To limit the number of chemical species in the fuse arc plasma the glass window can be replaced by a quartz window [35].

The specific fuse body with optical fibre inserted used by *Cheim* is shown in figure 6(a), the optical fibre being close to the fuse element reduced section (≈ 3 mm) and in front of its centre. From the measurement of the ratio between radiation intensities from various lines the temperature is deduced versus the *arcing* time. Temperature is obtained from the ratio of the intensities (ξ'/ξ) of emissions of radiation [39]: $\xi'/\xi = \left(\lambda^3 g f / \lambda'^3 g' f' \right) \times \exp[(E' - E) / k_B T]$ where λ is the wavelength, g the statistical weight of the line, f the oscillator strength, E the energy level. This formulation can also be written for lines corresponding to two consecutive ionization stages. From these formulations the temperature T identified to the plasma temperature is obtained for the whole duration of the *arcing* period: from Si II 505 nm and Si II 634 nm lines in figure 6(b) and from Si II 413 nm and Si III 457 nm in figure 6(c). From Si II lines the temperature decreases from $\sim 20\,000$ K down to $\sim 9\,000$ K, and from Si II and Si III lines the temperature decreases from $\sim 25\,000$ K down to $\sim 24\,000$ K during the first

millisecond of the *arcing* time, and increases weakly and steadily up to $\sim 26\,000$ K for ~ 3 ms. As it is mentioned by the authors themselves: the trend in figure 6(b) appears to be coherent with the fact that during the *arcing* period energy in the fuse decreases which justifies the cutting role played the fuse ; but the trend in figure 6(c) shows a mean value $\sim 25\,000$ K during the whole of the *arcing* period and even during the last millisecond of operation which seems to reinforced the measurements of *Chikata*. During this last millisecond current in the fuse falls quickly down to zero which appears to be in contradiction with the temperature measurement. Authors explain that the radiations emitted in the hot plasma core may be absorbed by colder layers located at the edges of the plasma column. These layers develop between the emission area of the studied transitions and the end of the optical fibre close to the edges of the interaction volume. They finally argue that for lines corresponding to high quantum levels the influence of absorption is negligible and that these lines can be considered as thin lines. First, narrow bandwidth filters are used to record only the part of radiation corresponding to the lines studied. The silicon lines used (Si II, and Si II and Si III) are sensitive to Stark broadening so the resulting full width at half maximum of these lines can be many nanometers of even tens of nanometers. This can be increased by the high level of continuous radiation, the observed spectrum being the result of the convolution of the Stark broadened profile with the continuum. Secondly, we can imagine that once the electric power is around its maximal value which falls approximately in the same time as maximum pressure, there exists a very strong gradient in material density from the core to the surroundings of the plasma column. As once more the Abel inversion is impossible to go back to local emissivities, the effect of these strong gradients can not be understood. Finally it is evident that the lack of the radial profiles of the silicon lines is a strong limitation which makes more difficult the temperature analysis from the recording of lines intensities.

Reliable comparisons are sometimes difficult to perform mainly because of the spectroscopic considerations linked to the various devices or whole experimental set-ups. For example in the past interferential filters were often used to obtain the spectral selectivity. At the present time CCD matrix with high sensitivity and high spectral resolution is commonly used. Considerations linked to intensity calibration are also of high interest but they are poorly discussed in the bibliography [40] and even less in the case of the electric fuse plasma analysis. On the contrary main of the electrical properties can be easier compared in so far as electrical features and fuse element features are accurately depicted. As a conclusion about the reliability and the reproductivity of the measurements dedicated to electric fuses one can conclude that reproducible measurements can be performed (especially owing to the improvement of technological solutions), the more questionable step lying in the analysis of the experimental results and the corresponding assumptions made to apply classical diagnostic methods such as in spectroscopic analysis.

The fuse arc plasma properties such as the temperature and the electron density i.e. microscopic properties can be directly linked to macroscopic properties such as the morphometric properties of the silica sand.

- Temperature of the fuse arc plasma is obtained by assuming a Boltzmann distribution for the energy levels [35, 38, 40] thus leading to the excitation temperature. If thermal equilibrium conditions are assumed one can identify the excitation temperature with the electron temperature (electron velocities following a Maxwell distribution). This method can be applied with integrated intensities (I_l) for the studied line (with spectral profile $P_l(\lambda)$) instead of local emissivities ($\varepsilon_{l\lambda}$) at the condition that the plasma can be considered as homogeneous along the line of sight (L) namely:
$$I_l = \int_{\lambda} I_{l\lambda} \cdot d\lambda = L \int_{\lambda} \varepsilon_{l\lambda}(\lambda) P_l(\lambda) d\lambda = L \times (1/4\pi) \times (hc/\lambda_{j,ul}) \times A_{j,ul} \times n_{j,k}$$
 (h : Planck constant, c : speed of light in vacuum, $\lambda_{j,ul}$: wavelength of line emitted by the j -chemical species where u and l symbolize the upper E_u and lower E_l energy levels of the transition, $A_{j,ul}$: transition probability of the line, and $n_{j,k}$ is the part of excited particles of the j -chemical species with $u, l \equiv k$). In the case of fuse arc plasma one can only work with integrated intensities

because the set of radial measurements necessary to obtain $\varepsilon_{I\lambda}$ from I_I (by Abel inversion) is impossible. The hypothesis for which homogeneity is considered valid along the line of sight is highly questionable. As a consequence it is better to consider the experimental temperature as an average temperature. In the case of the fuse arc plasma the assumption of the Boltzmann distribution for the energy levels and more generally about the Maxwell-Boltzmann distribution linked to equilibrium considerations is a complex task. Even in the case of apparent easier situations – such as plasma produced by ICP torch – some key points are still under consideration (see [40] for discussions about the accuracy of classical spectroscopic methods used to assess excitation temperature, electron temperature and the thermal disequilibrium). The high pressure level in the fuse arc plasma column is a favourable condition: in fact in the more general case of plasmas at least close to atmospheric pressure the number of collisions is sufficient for efficient energy transfer. As a consequence the Maxwellian distribution function is obtained for particles of the same species. As high level of electron density is obtained in the fuse arc plasma especially when the electric power is maximum [35], typically $\sim 10^{18} \text{ cm}^{-3}$, we can assume that the transfer of energy between electrons (e) and heavy particles (h) is efficient. Thus the unicity of temperature is assumed in order to define the plasma temperature by $T = T_e = T_h$. This unicity appears to be valid for the inner part of the plasma core where gradients (in temperature, density and pressure) are small (figure 8(c)) compared to the edges of the plasma. In the plasma surroundings the quoted gradients are strong and the composition of the plasma is continuously changed because of material injection (around the two erosion fronts and around the inner wall of the *fulgurite* or interaction volume). As a consequence the equilibrium assumption is difficult to assume for these areas. Local measurements could be helpful to analyse these areas, but typical methods such as Abel inversion can not be used. More details about the whole of these considerations linked to equilibrium (thermal, chemical) can be found in [64].

- Electron density of the fuse arc plasma is mainly obtained by means of two different approaches. First, it can be deduced by applying the Saha's equation [24] and using the experimental variation of the spectral intensities of various chemical species with different ionization degrees. This way is questionable in so far as the plasma composition has to be defined and LTE has to be assumed. Secondly, it is deduced from the spectral line shapes (broadening and sometimes shift) of ionized silicon lines by assuming that the observed spectral width at half maximum is mainly due to Stark broadening (splitting and shifting of the energy levels of the emitters) that is to say by pressure broadening [24, 30, 34, 35, 38]. So doing the assumption of LTE is not necessary. Main limitations lie in the subtraction of the continuous contribution and of the apparatus function. But in the analysis of the results one has to consider that even with ionized silicon lines the observed profile can be more or less broadened by absorption because of the radial gradients (in density, pressure and temperature).

2.3.3. Fulgurite. The formation of the *fulgurite* has been discussed in section 2.3 with quoted references in which more details can be found. This section is more concerned by the electric rigidity of the *fulgurite* once the *arcing* period is ended. It is of very high interest because the *fulgurite* has to ensure the highest dielectric rigidity possible to avoid any restriking linked to the appearance of a new electric *fault*.

In figure 7 we briefly illustrate some results from [41-43]. First in figure 7(a) is shown the dependence between the resulting resistance and the initial value of the copper fuse element thickness: higher values are obtained for thinner fuse elements. Secondly, as it has been previously observed in figures 5 and 11 (*Part I. Pre-arcing period*), there is a bulge located right at the initial position of the reduced section (linked to the high pressure which is the result of the metal vaporization). Each part of the *fulgurite* contributes in the resulting resistance. From figure 7(b) we see that the resistance obtained for the whole length of the *fulgurite* is especially the result of the contribution of the bulges: if the fuse element is equipped with many tens of reduced sections in series (typical case of an industrial fuse element) the resistance of the *fulgurite* will depend directly of these. Figure 7(c)

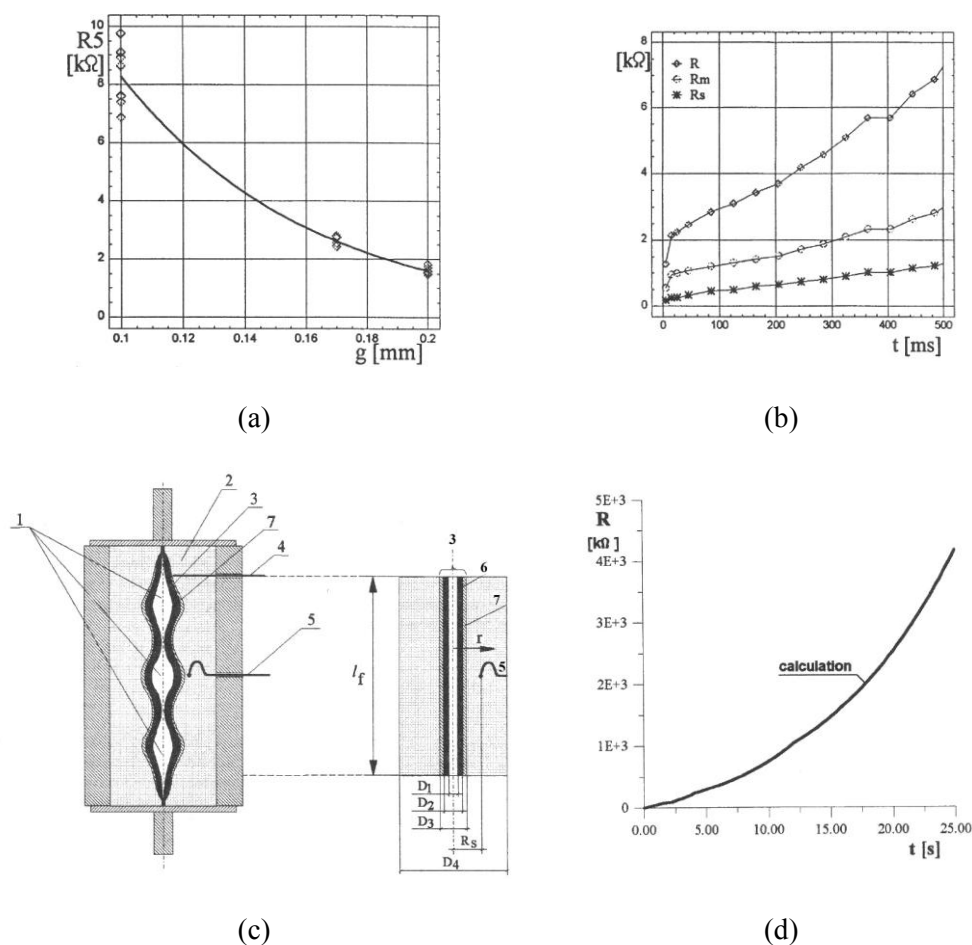


Figure 7. Considerations about the post-arc fulgurite resistance [41-43]. (a) Experimental post-arc resistance versus Cu element thickness (source voltage 500 V). (b) Distribution of post-arc resistance along different parts of fulgurite of Cu elements (resistances: R , for the whole length of the fulgurite; R_m , for only one metal part; R_s , for a swell of the fulgurite). (c) Sketches of the experimental fulgurite (on the left) and of the model put in the calculation: 1, swell observed at the initial place of the reduced section; 2, quartz sand; 3, fulgurite shell; 4, voltage probe; 5, thermocouple; 6, fully melted layer; 7, partially melted layer. (d) Profile of the fulgurite resistance versus time up to 25 s.

illustrates the simple schema retained to build the modelling: the actual fulgurite volume with bulges is simplified in an equivalent cylindrical volume. Especially fitted layers are deduced from a simple temperature cartography established by means of thermocouples inserted the filler volume, the temperature measurements being used to set the temperature profiles to put in the calculation. As a result we show in figure 7(d) the evolution of the post-arc resistance versus time. After few seconds a post-arc fulgurite resistance of some $k\Omega$ is obtained. Thus this simple tool can be helpful to design roughly the number of reduced sections and the gap between each of them.

2.4. Properties of the fuse arc plasma

Among the studies published up to know there are only a few numbers of papers dealing with the physico-chemical properties of the fuse arc plasma in spite of the fact that microscopic properties *i.e.*

those of the fuse arc plasma are of high interest in order to understand the macroscopic properties *i.e.* those induced by the fuse.

- At the microscopic scale. The transport coefficients of the fuse arc plasma – electrical conductivity, thermal conductivity, viscosity and radiation – are difficult to assess in an experimental way. From theoretical calculations [16, 17, 44-46] one knows that small variations of the metallic material to silica sand ratio can imply strong variations. Among them the fuse arc plasma radiation is the most studied even if few studies have been done. In that case the high difficulty lies in the analysis of the radiative properties especially for temperature and electron density measurements. To be obtained these evaluations require experimenters to apply classical spectroscopic methods whose assumptions and applicability are sometimes questionable. Some examples are detailed in the following sections.
- At the macroscopic scale. The analysis of the fuse resistance can be improved by use of the calculated electrical conductivity of the fuse arc plasma but many calculations are necessary to depict the whole duration of the *arcing* period and the whole of the plasma volume (for example of metallic type at the beginning and hence with an increasing percentage of silica). The instantaneous measurement of the pressure can be helpful at the condition that the measured pressure is the plasma pressure and that the plasma column shape is known at the time of evaluation [47]. The dimensional features of the fulgurite can be an indirect way to check the trends calculated for the viscosity but in this case the correlation has to be established from post-operation features (and the task is made more difficult because of the role played by the plasma pressure).

For physical modelling purposes of the *arcing* period one has to increase the knowledge of the physical processes occurring inside the plasma column. In the case of fuse arc plasma OES methods have led to the most significant contributions. In addition to the identification of the chemical species of the fuse arc plasma the temperature and electron density are obtained. As the fuse arc plasma radiation is assessed by means of an integration over the whole interaction volume thickness according to a single line of sight – whatever the way: either by direct insertion of an optical fibre either through a quartz window – the measured spectrum has to be considered as an average over this line of sight for the given integration time. This way to proceed raises many unknowns linked to fluctuations during the integration duration: about the changes in the plasma composition, about the optical thickness of the layers met by the light from the core of the plasma column to the surrounding layers where the light is collected, about the subvolume from which the studied spectroscopic line is emitted, about the validity of the necessary assumptions for the use of classical spectroscopic methods [40].

As example we show in figure 8(a) the spectra observed during the *arcing* period (*pre-arcing* time ~ 0.9 ms) for the spectral interval [360-440] nm. Neutral and ionized silicon lines are observed together with the continuum whose level changes significantly: sharp increase up to ~ 1.7 ms (for which electric power is maximum) followed by a regular decrease down to the end of the *arcing* period. The pressure evolution follows the electric power during *arcing* period [48]: thus for the time interval where the pressure level is high the lines used for temperature and electron density assessments are strongly broadened and the line wings are strongly disturbed. In the same time the level of the continuum increases and even becomes higher than the discrete radiation level: as a consequence discrete radiation becomes weaker compared to continuous radiation and can not be used any more for diagnostic purposes. In figure 8(b) we show a comparison between an experimental spectrum focussed on the ionized silicon multiplet Si II (2) and the calculated profiles for the two lines of the multiplet, namely ~ 634.7 nm and 637.1 nm and assuming a 100% SiO₂ plasma. This spectrum is observed ~ 3.24 ms after the application of the fault current, that is to say at the end of the *arcing* period for which the continuum level is low. Calculated profiles are obtained by means of the radiative transfer equation [36] written for only one dimension comparable to the line of sight. The observed

intensity I_λ is defined by:
$$I_\lambda(R) = \int_0^R \varepsilon_\lambda(x, T) \cdot \exp\left(-\int_x^R k_\lambda(x', T) dx'\right) dx$$
, where R indicates the

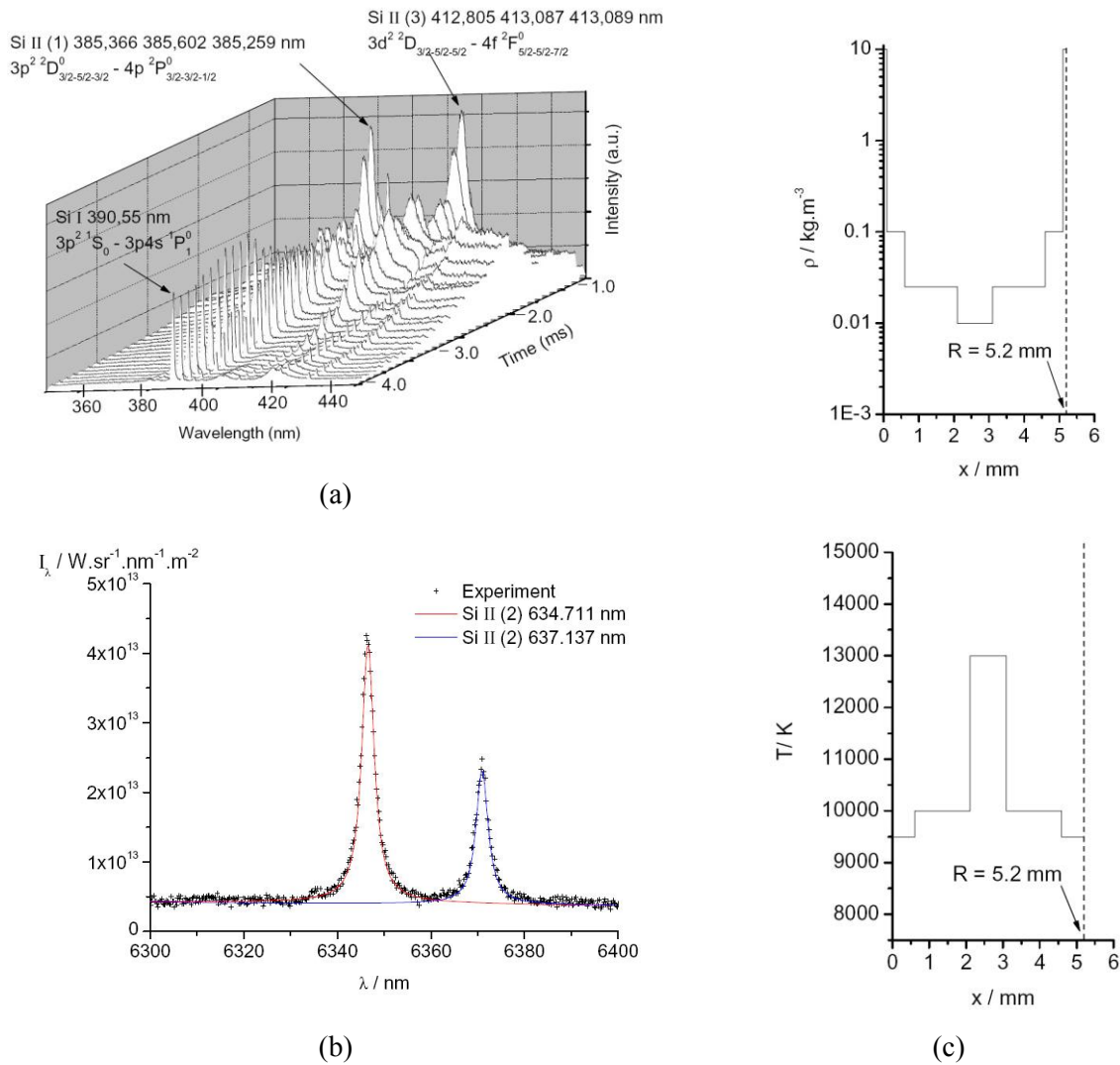


Figure 8. Fluctuations of the fuse arc plasma radiation [36]. (a) Evolution versus *arcing* time of the neutral silicon line Si I 390 nm and the two ionized silicon multiplets Si II (1) and Si II (3). (b) Experimental spectrum at 3.24 ms focussed on the Si II (2) ionized silicon multiplet. (c) Radial density and temperature deduced from the Radiative Transfer Equation.

edge of the integration domain, k_λ is the spectral absorption coefficient (necessary to calculate the optical thickness of the plasma at the wavelength λ) and the total spectral emissivity is: $\epsilon_\lambda(\lambda, T) = \epsilon_{j,ul,\lambda}(\lambda, T) + \epsilon_{fb,\lambda,j}(\lambda, T) + \epsilon_{ff,\lambda,j}(\lambda, T)$, where ϵ_{fb} and ϵ_{ff} are respectively the *free-bound* and the *free-free* contributions of the continuum. For this calculation the radial density and temperature of the plasma are shown in figure 8(c): the plasma density is weak in the center $\sim 0.01 \text{ kg}\cdot\text{m}^{-3}$ and increases up to ~ 1 to $10 \text{ kg}\cdot\text{m}^{-3}$ at the edges ; the maximum temperature is $\sim 13 \text{ kK}$ in the plasma core and decreases down to $\sim 9.5 \text{ kK}$ at the edges.

Spectroscopic considerations on one hand, and composition and transport coefficients calculations [46, 49-51] on the other hand are currently improved. For the latter the non equilibrium plasmas are studied in the low temperature domain namely from 1000 K to 6000 K. In addition to these novel calculation tools some experimental works have been done to study chemistry considerations linked to the *arcing* period in a fuse [23, 52, 53]. Especially in [23] experiments performed after the device

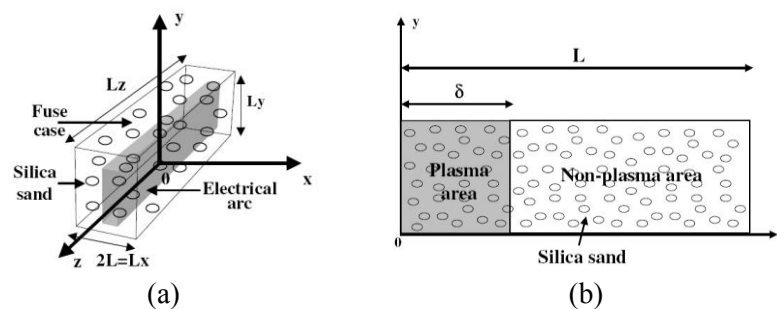


Figure 9. (a) Sketch of the geometry of the studied fuse. (b) Sketch of the one-dimensional geometry of the fuse process. From [57].

operation do not show any significant evidence of the lasting chemical change. The devices concerned are fast-acting HBC fuses with silver fuse elements designed to protect semi-conductor devices. Experiments include calorimetry, ‘wet’ analysis of the fuse fulgurite, electron spectroscopy for chemical analysis and determination of gas produced. On the whole of the results and within the range of experimental error no specific trend is pointed out from the chemical point of view and the results doesn’t show any permanent chemical change due to the fuse operation. Moreover the black regions that can be seen in figure 11 (*Part 1. Pre-arcing period*) have been analysed also and three main conclusions are given [23]: (a) the presence of silver oxide is not proved in significant quantities, (b) the central black area of the fulgurite corresponds to silicon dioxide (SiO_2) and silver, and hence (c) there is no evidence of lasting chemical change.

The distribution of silver within the fulgurite has been studied in [53] by means of local neutron activation. Results have been averaged over tens of fulgurites obtained after fuse operation and show that an axial flow of silver exists from the centre of the fulgurite towards the extremities, the anode side flow being stronger than the cathode side flow.

2.5. Trends in arcing period modelling

Most of the published works up to now are digital simulations [9, 10, 54] or more or less empirical calculations especially the one of *Daalder* [18] which is very comprehensive. Among digital simulations reliable calculations have been produced to predict current and voltage induced by the fuse but they are dependant on fitting paramaters *i.e.* specific to one type of fuse or based on simplifying geometrical considerations especially for the plasma column. One of the main difficulty to build a physical modelling is first to identify the physical processes that have to be included. This task is complex because the whole of the processes are not known or not known with acceptable accuracy to be depicted properly. Secondly one has to integrate the three phases for the materials with different silver to silica proportions, the ratio between each of these phases varying during the *arcing* period (due to the localization within the interaction volume). Thirdly the chemical species forming the fuse arc plasma can vary with the proportion of the material and with the level of pressure (the increase of pressure shifts the chemical reactions to the high temperatures). Fourthly the whole interaction volume is not delimited by a homogeneous and steady boundary with accurate limits. On the contrary the thickness of the melted silica layer surrounding the plasma column is inhomogeneous in temperature and most probably in density and viscosity. The diffusion of the melted silica and of the vapours produced in the plasma column has to be depicted because it corresponds to energy withdrawal and it modifies the whole electrical conductivity of the plasma column and of the electric fuse. And fifthly one has to find experimental and calculated or modelised quantities to establish reliable comparisons.

A physical modelling of the *arcing* period in a HBC fuse has been published in [55-58]. We invite to refer to these works to obtain the full mathematical and physical considerations included in themodelling. In the next parts only the quantities which can be compared with experiments are discussed.

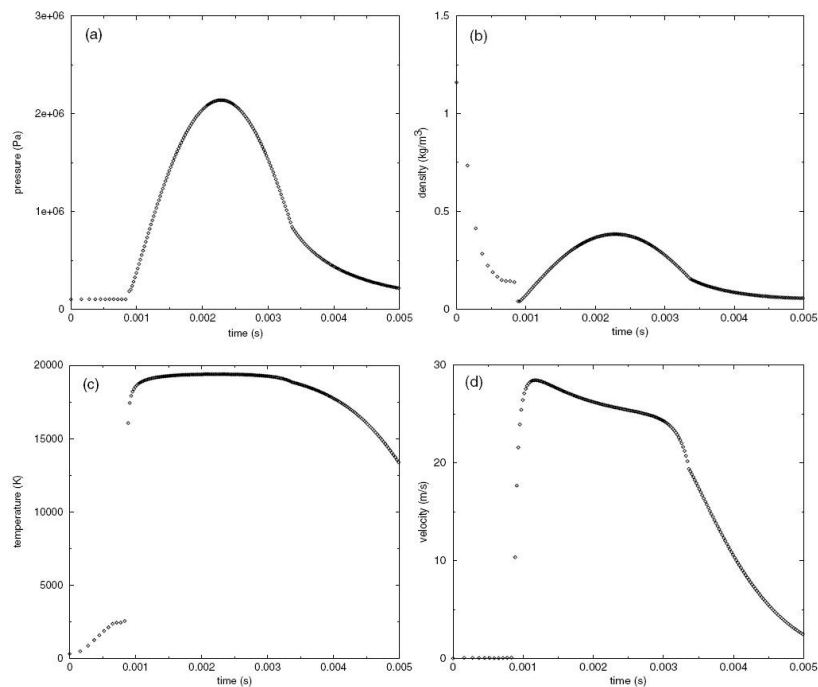


Figure 10. Pressure (a), density (b), temperature (c) and velocity (d) distributions in the plasma core during the fuse operation of 5 ms duration [57].

One of the contributions of these latter works is the approach developed to take into account the fluid flow through the porous granular filler. The sketch of the studied electric fuse is shown in figure 9(a) together with the one-dimensional geometry retained for the modelling. To simplify the fuse domain is divided into two main areas, the plasma area and the silica sand area. To model the HBC fuse the compressible Euler equations for perfect gas are used. The basic flow model is coupled with a model of the porous medium which integrates a mechanical interaction between the gas and the silica sand and the heat transfer between the hot gas and the cold silica sand grains. From the numerical point of view a finite volume scheme is used and each cell is defined according to the material involved depending on the area: especially in the silica sand the void space filled with air is set by the porosity ϕ whereas the silica sand correspond to $(1-\phi)$. The fluid flow through the porous filler is described by means of the Darcy and Forchheimer coefficients experimentally assessed by means of a modified Ergun's equation [59,60] where the pressure drop (ΔP) through the porous layer of given thickness (L) is given as a function of the fluid velocity (v) by: $\Delta P/L = (\mu v)/k_1 + (\rho v^2)/k_2$, k_1 is the viscous term linked to the Darcy coefficient and k_2 is the inertial term linked to the Forchheimer coefficient. Mass, momentum and energy conservations are written and the heat transfer is described by taking into account the effective thermal conductivity of the filler. In figure 10 we show the evolutions versus time of the pressure, the density, the temperature and the velocity in the plasma core for total fuse operation of 5 ms, the *pre-arc*ing period duration is ~ 0.9 ms. The pressure increases quickly up to ~ 2.2 MPa at ~ 2.3 ms before to decrease steadily down to nearly atmospheric pressure. The plasma temperature shows a sharp increase at the beginning of the *arc*ing period up to $\sim 20\,000$ K and remains nearly unchanged up to ~ 3 ms, the temperature at 5 ms being $\sim 13\,000$ K. The density normally falls from ~ 1 kg·m $^{-3}$ at the beginning of the *pre-arc*ing time to less than 0.1 kg·m $^{-3}$ at the beginning of the *arc*ing time. Next it increases due to vaporization of material and high temperature and reaches ~ 0.4 kg·m $^{-3}$ when the pressure is maximum and finally decreases down to less than 0.1

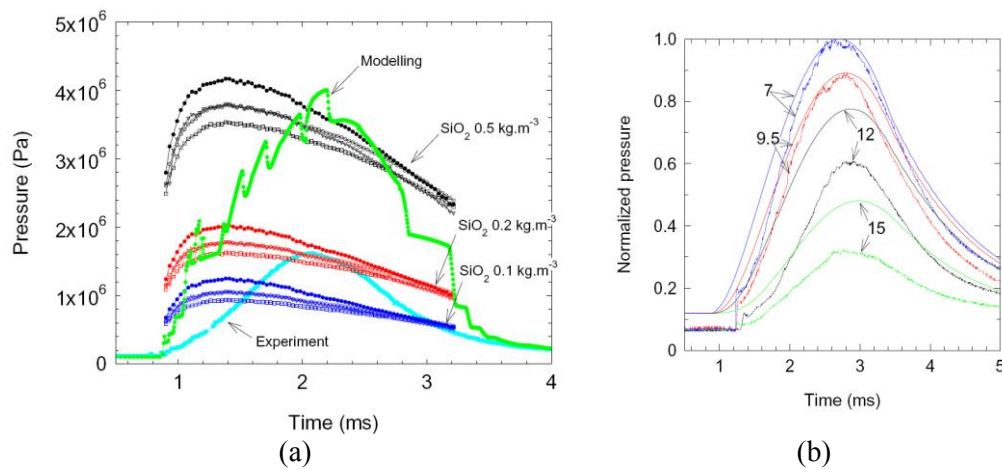


Figure 11. (a) Evolution of the pressure during the fuse operation [36]: comparison between experiments [48], simulations from modelling [57] and calculations (for three initial SiO₂ amounts fully vaporized to form the fuse arc plasma) [17]. (b) Comparison between experiments and simulations given in normalized pressure: at 7 mm, 9.5 mm, 12 mm and 15 mm from the initial position of the fuse strip [61].

kg.m⁻³ at the end of the *arc*ing period. More simulations can be found in [57] at different positions (at the plasma periphery ~ 1 mm and in the filler) which exhibit coherent trends.

The fuse arc plasma pressure is one of the physical quantities which can be compared (figure 11). Experimental curves shown in figure 11(a) are similar to those showed in figure 9(b) (*Part 1. Pre-arc*ing period): they correspond to the pressure measured the closest as possible of the plasma column within the granular filler for a given experimental test [48]. Simulated pressure is the arc plasma pressure obtained in the same way as in figure 10 but for different conditions corresponding to the experimental tests. Calculated pressures are given for three silica plasma compositions namely 0.1 kg.m⁻³, 0.2 kg.m⁻³ and 0.5 kg.m⁻³: for each case three curves are given depending on the temperature scale which is deduced from the spectroscopic measurements [36]. The experimental and simulated pressures follow a similar trend, the simulation (arc plasma pressure) showing logically higher values compared to experiments (pressure within the solid silica sand but the closest as possible to the plasma edges). On the contrary and whatever the composition, calculated pressures exhibit a significantly different trend. These latter are obtained from the temperature/time correlation for each of the plasma compositions. The absorption of the radiation emitted in the plasma core by the colder surrounding plasma layers justifies partially these different trends.

From the calculation of the Darcy and Forchheimer contributions the total flow resistance can be calculated [48, 57, 58] and the variation of the pressure during the fuse operation can be deduced at various positions from the fuse element and compared with measurements [61]. The comparison is shown in figure 11(b) in terms of normalized pressure for the following positions from the initial position of the fuse element: 7 mm, 9.5 mm, 12 mm and 15 mm (absolute measurements can be found in [61]). For the smallest value *i.e.* 7 mm the sensitive area of the quartz pressure transducer is very close to the edges of the fulgurite (a closer position could imply irreversible damages for the piezoelectric transducer). A good agreement is found about the time variation especially for the closest positions 7 mm and 9.5 mm. For 12 mm and 15 mm there are some reasonable discrepancies between measurement and simulation. This is due to the higher silica sand thickness. The pressure wave ignited in the plasma column is transferred via the silica sand grains intersection points: higher the silica sand thickness, higher the number of intersection points and stronger the reduction of the pressure wave magnitude.

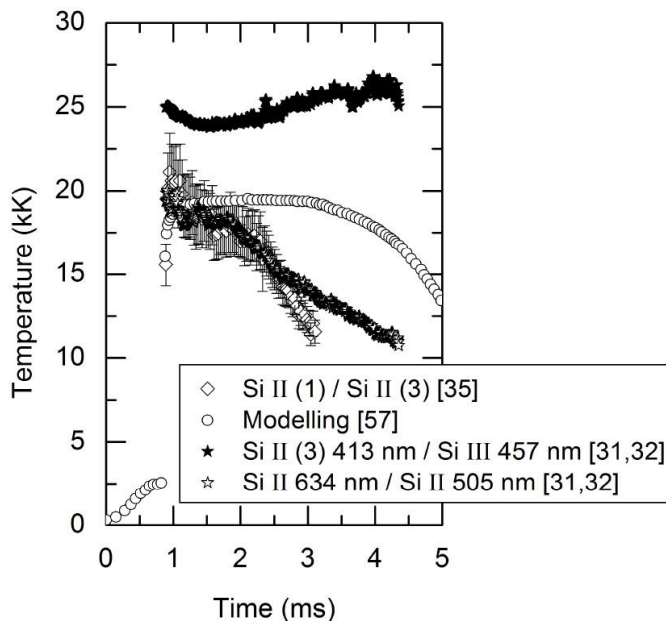


Figure 12. Comparison of various fuse arc plasma temperature values from experiments and modelling: M , average excitation temperature with uncertainties bar from Si II (1) and (3) multiplets [35]; \circ , simulated temperature [55,57]; ψ , plasma temperature from Si II (2) 634 nm / Si II 505 nm ratio [31,32]; ξ , plasma temperature from Si II (3) 413 nm / Si III 457 nm ratio [31,32]. For ψ and ξ , the initial time scale referring to the *arc*ing time only is shift ~ 0.9 ms to be compared.

In figure 12 we show a comparison between the fuse arc plasma temperatures obtained in various ways. For a given mean granulometric interval [35] the mean excitation temperature is obtained from the relative intensity ratio method with the multiplets (1) and (3) of ionized silicon. The temperature increases from ~ 15.5 kK (the first spectrum during the *arc*ing period is obtained ~ 30 μ s after the arc ignition) to ~ 21 kK at the most. Hence the temperature decreases less or more regularly down to ~ 12 kK for ~ 3.1 ms (spectra integrated up to the cancellation of current can not be used for spectroscopic diagnostic). Up to ~ 2 ms these measurements are close to the simulated temperature [55, 57] especially as uncertainty bars are considered. Significant discrepancies appear after 2 ms of operation. Simulated temperatures are roughly unchanged up to ~ 3.2 ms and hence decrease steadily down to ~ 13.5 kK at 5 ms. First noticeable inhomogeneity appears from the plasma core towards the plasma edges thus changing the optical thickness of the ionized silicon lines along the line of sight and increasing the broadening of the ionized silicon lines by absorption. Secondly the spreading of melted silica through the pores of the filler is omitted in the modelling thus an energy loss term is omitted and this remaining energy corresponding to the whole hot plasma energy is overestimated. The temperatures obtained by means of spectroscopic measurements with Si II lines by *Cheim* [31, 32] are consistent with those of [35]. On the contrary the temperatures deduced from the relative intensity ratio method with Si II and Si III lines are quite stable with a rough mean value ~ 25 kK. A significant increase is observed after 2 ms which is inconsistent with the decrease of the energy provided to the fuse plasma. Considerations linked to optical thickness and absorption due to radial gradients could explain this trend.

From temperature [24, 29] and electron density [24, 30, 61] measurements the electron density versus temperature curves can be obtained for the whole duration of the fuse operation. An example is shown in figure 13 and compared with electron densities calculated for various SiO₂ plasmas (volume is kept constant): $0.1 \text{ kg}\cdot\text{m}^{-3}$, $0.2 \text{ kg}\cdot\text{m}^{-3}$, $0.5 \text{ kg}\cdot\text{m}^{-3}$ and $1 \text{ kg}\cdot\text{m}^{-3}$. It can be noticed that in the temperature range from ~ 16.5 kK to ~ 18.5 kK the assessment of electron density is not possible. This temperature domain is obtained when the electric power is at its maximum level. For these conditions the level of continuous radiation is the highest observed during the fuse operation and it is not possible to observe the ionized silicon lines any more: the radiation emitted in the plasma core crosses dense layers in the radial direction towards the plasma edges as shown in figure 8(c). From the calculated curves shown in figure 13 one notes that a single calculation is not sufficient to describe the fuse

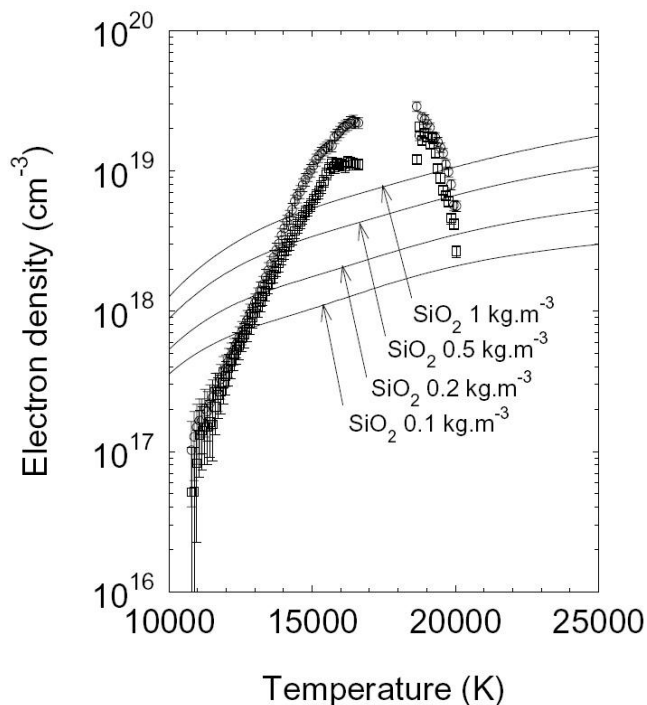


Figure 13. Electron density curves $n_e(T)$ [61]: comparison between experiments (Stark broadening of Si II (2) multiplet: ∇ , 634 nm and \square , 637 nm) and composition calculation for SiO₂ plasma.

operation. Actually the evolution of the fuse arc plasma electron density is the result of the variation of the plasma composition: of metallic type at the beginning of the *arcing* period and of silica type for most of the *arcing* period duration. The electron density shown in figure 13 lies varies from $\sim 10^{17} \text{ cm}^{-3}$ to $\sim 10^{19} \text{ cm}^{-3}$. These values and the trends during the *arcing* period depend strongly on the morphometric properties of the silica sand.

3. Conclusion

The *arcing* period is clearly more complex to describe and to model compared to the *pre-arcing* period (*Part 1. Pre-arcing period*). The assessment of the fuse arc plasma properties is mainly done by means of classical spectroscopic diagnostics whose applicability is sometimes difficult to justify. Especially conditions to obtained LTE within the plasma core can be reasonably assumed. On the contrary for the area where the arc is ignited and for the edges of the fuse arc plasma the LTE assumption appears questionable and the changes in the plasma composition (both close to the erosion front and close the plasma edges) are still unknown. The plasma core – high temperature, electron density and pressure and low density – is surrounded by colder layers whose composition changes during the *arcing* period and with distance from the plasma core. These various temporal and spatial gradients imply strong inhomogeneities and absorption of the radiation issued for the hottest areas of the fuse arc plasma. The knowledge of the plasma properties has to be increased to identify the physical processes in order to build a comprehensive modelling.

Acknowledgments

The author is grateful to industrial partners and academic partners for their useful discussions and their help during continued collaborations (Alstom, Electricité de France, Schneider Electric, Mersen, ACOIFF, Direction Générale des Entreprises) and also to J Aubretton and MF Elchinger from SPCTS Limoges. The author would like to thank particularly the colleagues from LAEPT.

References

- [1] Lefort A 1998 Questions about arc roots ? *Invited lecture. XIIIth Symp. on Phys. Switching Arc* (Brno 7-11 Sept. 1998)

- [2] Abbaoui M and Lefort A 2009 Arc root interaction with the electrode: a comparative study of 1D-2D axi symmetric simulations *Eur. Phys. J. Appl. Phys.* **48** N°1 11001
- [3] Jüttner B 2001 Cathode spots of electric arcs *J. Phys. D: Appl. Phys.* **34** R103-123
- [4] Benilov MS 2002 Theory and modelling of arc cathodes *Plasma Sources Sci. Technol.* **11** A49-54
- [5] Heberlein J, Mentel J and Pfender E 2010 The anode region of electric arcs: a survey *J. Phys. D: Appl. Phys.* **43** 023001
- [6] Shkol'nik SM 2011 Anode phenomena in arc discharges: a review *Plasma Sources Sci. Technol.* **20** 013001
- [7] Lefort A and Andanson P 1985 Characteristic parameters of the anode spot *IEEE Trans. on Plasma Science* **13** N°5 296-299
- [8] Wright A and Newbery P G 2004 Electric fuses ed IEE Power & Energy Series **49** 3rd edition (London)
- [9] Wright A and Beaumont KJ 1976 Analysis of high-breaking-capacity fuselink arcing phenomena *Proc. IEE* **123** N°3 pp 252-258
- [10] Gnanalingam S and Wilkins R 1980 Digital simulation of fuse breaking tests *Proc. IEE* **127** C 6 pp 434-440
- [11] Reineri CA, Gomez JC and Magnago F 1993 Experimental determination of fuse filler thermal conductivity 7th Int. Conf. on Switching Arc Phenomena (Lodz, Poland) **Part I** pp 220-223
- [12] Bussière W 2001 Estimation of the burn-back rate in high breaking capacity fuses using fast imagery *J. Phys. D: Appl. Phys.* **34** 1007-1016
- [13] Jabubiuk K and Lipski T 1993 Dynamics of fulgurite formation during arcing in HRC fuses *J. Phys. D: Appl. Phys.* **26** 424-430
- [14] Sloot JGJ, Kalasek VKI and Sikkenga J 1987 *A one dimensional mathematical model for the dynamical burnback velocity of silver strips* *Proc. of the 3rd Int. Conf. on Electric Fuses and their Applications* (ICEFA Eindhoven Netherlands) pp 72-77
- [15] Fauchais P 2005 *Plasmas thermiques : aspects fondamentaux* ed Techniques de l'Ingénieur **D 2810**
- [16] André P, Bussière W and Rochette D 2007 *Transport coefficients of Ag-SiO₂ plasmas* *Plasma Chem. Plasma Process* **27** pp 381-403
- [17] Bussière W and André P 2001 *Evolution of the composition, the pressure, the thermodynamic properties and the monoatomic spectral lines at fixed volume for a SiO₂-Ag plasma in the temperature range 5000-25 000 K* *J. Phys. D: Appl. Phys.* **34** pp 1657-1664
- [18] Daalder J A, Schreurs E F 1983 *Arcing phenomena in high voltage fuses* EUT Report **83-E-137** (Eindhoven: EUT Dept. of Electrical Engineering)
- [19] Wilkins R and Gnanalingam S 1978 *Burn-back rates of silver fuse elements* *Proc. of the 5th Int. Conf. on Gas Discharges* (University of Liverpool) pp 195-198
- [20] Turner HW and Turner C 1977 *Calculation of the burn-back rate of a fuse element and its relation to contact erosion* *Proc. of the 3rd Int. Symp. on Switching Arc Phenomena* (Lodz, Poland) pp 334-337
- [21] IEC 60282-1, ed 5: High-voltage fuse – Part 1: Current-limiting fuses, International Electrotechnical Commission, 2002
- [22] Lakshiminarashima CS, Barrault MR and Oliver R 1978 *Factors influencing the formation and structure of fuse fulgurites* *Proc. IEE* **125** 5 391-399
- [23] Barrow DR, Howe AF and Cook N 1991 *The chemistry of electric fuse arcing* *IEE Proc.-A* **138** 1 pp 83-88
- [24] Chikata T, Ueda Y, Murai Y and Miyamoto T 1976 *Spectroscopic observations of arcs in current limiting fuse through sand* *Proc. Int. Conf. On Electric Fuses and their Applications* (Liverpool, UK) 114-121
- [25] Saqib M and Stokes AD 1999 *Time resolved spectrum of the fuse arc plasma* *Thin Solid Films* **345** 151-155

- [26] Stokes AD, Sibilski H and Kovitya P 1989 *Ablation arcs. II. Arcs in plastic materials and in boric acid* J. Phys. D: Appl. Phys. **22** **11** 1702-1707
- [27] Cao LJ and Stokes AD 1991 *Ablation arc. III. Time constants of ablation-stabilized arcs in PTFE and ice* J. Phys. D: Appl. Phys. **24** **9** 1557-1562
- [28] Cao LJ and Stokes AD 1992 *Ablation arc. IV. Spectrum analysis of the ablation-stabilized arcs in ice* J. Phys. D: Appl. Phys. **25** **4** 669-676
- [29] Saqib MA, Stokes AD, James BW and IS Falconer 1999 *Arc temperature measurement in a high-voltage fuse* Proc. of the 6th Int. Conf. on Electric Fuses and their Applications (Torino, Italy) 107-110
- [30] Saqib MA, Stokes AD, James BW and Falconer IS 1999 *Measurement of electron density in a high-voltage fuse arc* Proc. of the 6th Int. Conf. on Electric Fuses and their Applications (Torino, Italy) 129-132
- [31] Cheim LAV 1992 *Arc temperature measurements in high breaking capacity fuses* Ph.D Thesis, University of Nottingham, Department of Elect. and Electronic Engineering
- [32] Cheim LAV and Howe AF 1994 *Spectroscopic observation of high breaking capacity fuse arcs* Proc. IEE Sci. Meas. Technol. **141** 123-128
- [33] Barrow DR and Howe AF 1991 *The use of optical spectroscopy in the analysis of electric fuse arcing* Proc. of the 4th Int. Conf. on Electric Fuses and their Applications (ICEFA, Nottingham, UK) pp 221-225
- [34] Bussière W and Bezborodko P 1999 *Measurements of time-resolved spectra of fuse arcs using a new experimental arrangement* J. Phys. D: Appl Phys. **32** **14** 1693-1701
- [35] Bussière W 2001 *Influence of sand granulometry on electrical characteristics, temperature and electron density during high-voltage fuse arc extinction* J. Phys. D: Appl. Phys. **34** **6** 925-935
- [36] Bussière W, Rochette D, André P, Velleaud G and Memiaghe S 2007 *Study of the SiO₂ plasma radiation. Application to the fuse arc plasma* Proc. of the 8th Int. Conf. on Electric Fuses and their Applications (ICEFA, Clermont-Ferrand, France) ed Blaise Pascal University Press p 109-119
- [37] Arai S 1999 *Geometrical model of discharge space in the state of the high arc voltage generation of capillary arcs* Proc. of the 6th Int. Conf. on Electric Fuses and their Applications (Torino, Italy) 119-124
- [38] Bussière W 2000 *Mesure des grandeurs (T, Ne, P) au sein du plasma d'arc des fusibles en moyenne tension* Ph. D Thesis (in French) Université Blaise Pascal **DU 1258** EDSF **301**
- [39] Griem H 1964 *Plasma spectroscopy* ed McGraw-Hill
- [40] Bussière W, Vacher D, Menecier S and André P 2011 *Comparative study of an argon plasma and an argon copper plasma produced by an ICP torch at atmospheric pressure based on spectroscopic methods* **20** **4** 23pp
- [41] Cwidak K and Lipski T 1993 *Post-arc resistance in HBC fuses* Proc. of the 7th Int. Conf. on Switching Arc Phenomena (TU Lodz, Poland) pp 202-205
- [42] Cwidak K and Lipski T 1995 *New results on the post-arc fulgurite resistance of HBC fuses* Proc. of the 5th Int. Conf. on Electric Fuses and their Applications (ICEFA, Ilmenau, Germany) pp 219-222
- [43] Jakubiuk K and Cwidak K 1995 *Analytical model of post-arc fulgurite resistance of HBC fuses* Proc. of the 5th Int. Conf. on Electric Fuses and their Applications (ICEFA, Ilmenau, Germany) pp 223-228
- [44] André P 1995 *Etude de la composition et des propriétés thermodynamiques des plasmas thermiques à l'équilibre et hors d'équilibre thermodynamique* Ph. D Thesis (in French) Université Blaise Pascal **DU 771** EDSF **85**
- [45] Rochette D, Bussière W and André P 2004 *Composition, enthalpy, and vaporization temperature calculation of Ag-SiO₂ plasmas with air in the temperature range from 1000 to 6000 K and for pressure included between 1 and 50 bars* Plasma Chemistry and Plasma Processing **24** **3** pp 475-492

- [46] André P, Aubreton J, Bussière W, Elchinger MF, Memiaghe S and Rochette S 2007 *Basic data: composition, thermodynamic properties and transport coefficients applied to fuse* Proc. of the 8th Int. Conf. on Electric Fuses and their Applications (ICEFA, Clermont-Ferrand, France) ed Blaise Pascal University Press pp 95-100
- [47] Bussière W, Duffour E, André P, Pellet R and Brunet L 2004 *Experimental assessment of temperature in plasma wall interaction* Eur. Phys. J. D **28** pp 79-90
- [48] Rochette D and Bussière W 2004 *Pressure evolution during HBC fuse operation* J. Phys. D: Appl. Phys. **13** pp 293-302
- [49] Koalaga Z and Zougmore F 2003 *Composition of CxHyOzNt plasmas out of thermal equilibrium using quite different modified forms of Saha and Guldberg-Waage equations* IEEE Trans. on Plasma Science **31** 1 pp 82-93
- [50] André P and Koalaga Z 2010 *Composition of a thermal plasma formed from PTFE with copper in non-oxidant atmosphere. Part I: definition of a test case with the SF6 JHTMP* **14** 3 pp 279-288
- [51] André P and Koalaga Z 2010 *Composition of a thermal plasma formed from PTFE with copper in non-oxidant atmosphere. Part II: comparison of a test case with nitrogen JHTMP* **14** 3 pp 289-296
- [52] Wasserman AA, Melosh HJ, Laurretta DS 2002 *Fulgurites: a look at transient high temperature processes in silicates* Proc. of the 33rd Lunar and Planetary Sc. Conf. (LPSC, Texas, US) **1308** 2pp
- [53] Murin-Borel V, Lieutier M, Parizet MJ, Barrault M, Melquiond S, Rambaud T and Vérité JC 2000 *Silver mass flow in high-voltage fuses* J. Phys. D: Appl. Phys. **33** 6 pp 753-756
- [54] Wilkins R and McEwan PM 1975 *A.C. short-circuit performance of notched fuse elements* Proc. IEE **122** 3 289-292
- [55] Rochette D 2002 *Modélisation et simulation de la décharge d'arc électrique dans un fusible moyenne tension* Ph. D Thesis (in French) Université Blaise Pascal **DU 1400** EDSF **372**
- [56] Rochette D and Clain S 2003 *Numerical simulation of Darcy and Forchheimer force distribution in a HBC fuse* Transport in Porous Media **53** pp 25-37
- [57] Rochette D and Clain S 2004 *Mathematical model and simulation of gas flow through a porous medium in high breaking capacity fuses* Int. J. of Heat and Fluid Flow **25** pp 115-126
- [58] Rochette D and Clain S 2004 *Local heat transfer of compressible fluid in porous media: application to the HBC fuse* Int. J. of Heat and Fluid Flow **26** pp 322-333
- [59] Bussière W, Rochette D, Latchimy T, Velleaud G and André P 2006 *Measurement of Darcy and Forchheimer coefficients for silica sand beads* High Temp. Mat. Processes **10** pp 55-78
- [60] Ergun S 1952 *Fluid flow through packed columns* Chem. Eng. Progress **48** 2 pp 89-94
- [61] Bussière W, Rochette D and Pellet R 2003 *Influence of the filling material properties on the pressure in HBC fuse. Comparison between experimental results and simulation* Proc. of the 7th Int. Conf. on Electric Fuses and their Applications (ICEFA, Gdansk, Poland) pp 111-118
- [62] Ranjan R and Barrault MR 1980 *Axial electric-field measurements of d.c. arcs in current-limiting fuses* IEE Proc. **127** C 3 pp 199-202
- [63] Murin-Borel V 1999 *Fusibles en moyenne tension : détermination des mécanismes physiques de fonctionnement* Ph. D Thesis (in French) Université Blaise Pascal EDSPIC
- [64] Rat V, Murphy AB, Aubreton J, Elchinger MF and Fauchais P 2008 *Treatment of non-equilibrium phenomena in thermal plasmas* J. Phys. D: Appl. Phys. **41** 28pp